Theor Chem Acc (2010) 127:1–17
DOI 10.1007/s00214-010-0760-4

FEATURE ARTICLE

Wavepacket quantum dynamics

Gabriel G. Balint-Kurti

Received: 24 February 2010 / Accepted: 16 April 2010 / Published online: 12 May 2010

Abstract The article reviews the use of wavepackets in molecular quantum dynamics. The basic theory concerned with their use in both reactive molecular scattering and photodissociation dynamics is outlined. The great advantage of using wavepackets is that the full **S** matrix for the scattering problem need not be evaluated, and the numerical effort can be concentrated on those initial molecular quantum states which are of interest. Wavepackets may be used within a time-dependent or a time-independent framework, both are discussed and compared. Some examples of calculations from both reactive scattering and photodissociation theory are given.

Keywords Wavepackets · Quantum mechanics · Molecular dynamics · Molecular collisions · Reactive scattering · Photodissociation

1 Introduction

The first quantum mechanical time-dependent wavepacket treatment of a collinear reactive scattering process was published by Mazur and Rubin [1] in 1959 and was followed by several further investigations [2–8]. These early works were not however actively pursued and for a period after this time-independent treatments of quantum reactive scattering were intensively and almost exclusively developed and used [9–15].

Starting in 1978 Heller and co-workers published a series of important articles using a time-dependent wavepacket approach to calculate photodissociation cross sections and Raman spectra [16–19]. While some exact, two mathematical dimensional calculations were described in these early works, [20] including the evaluation of product quantum state distributions, the main emphasis was on semi-classical methods of solving photodissociation dynamics. This work has been developed to great effect by several groups who have applied it extensively to the photochemistry of large systems [21–24]. Other groups have used exact quantum dynamics to describe the motion of some atoms in a large system while using classical mechanics to describe the motion of other atoms [25, 26]. In the present paper we will not discuss these semiclassical or mixed quantum classical methods, but will rather concentrate on the use of exact quantum dynamical methods.

Important breakthroughs in the application of quantum wavepacket dynamics were first the introduction of grid-based Fourier transform methods [27–29], which permitted the rapid evaluation of the action of the Hamiltonian operator on the wavepacket and secondly the introduction of the highly efficient Chebyshev expansion [30–32] of the time-evolution operator, which greatly increased the accuracy of the solution of the time-dependent Schrödinger equation. As we will see below later developments of this method permitted the introduction of various even more efficient time-independent wavepacket approaches, which use the iteration number of the Chebyshev expansion to replace the time variable.

Molecular quantum mechanical scattering calculations are extremely demanding on computational resources. Wavepacket approaches make the calculations greatly more efficient because they are initial value problems [33] and therefore only solve one column of the **S** matrix at a time, concentrating numerical effort on those initial states which may be populated in the experimental situation of interest.

G. G. Balint-Kurti (✉)
Centre for Computational Chemistry, School of Chemistry, University of Bristol, Bristol BS8 1TS, UK
e-mail: Gabriel.Balint-Kurti@Bristol.ac.uk

Several recent reviews of quantum wavepacket dynamics have been published [34–41]. This article will outline the application of wavepacket dynamics to reactive scattering and photodissociation theory.

2 Time-dependent versus time-independent formulation

The quantities of interest in photodissociation and reactive scattering, such as cross sections, are always functions of the energy or frequency, rather than of time. As time and energy are canonically conjugate variables [42] the quantities dependent on them are related by Fourier transforms, in the same way as are coordinate and momentum wavefunctions [43, 44].

In order to illustrate the relationship between the time-dependent and the time-independent formulations we consider the total photodissociation cross section for a triatomic molecule [16, 36].

We can write the total photodissociation cross section as:

$$\sigma_{tot}(E) = \frac{2\pi^2 v}{c\epsilon_0} \sum_{vjm_j} \int \mathrm{d}\hat{\mathbf{k}} |\langle \psi^-_{vjm_j}(\mathbf{r}, \mathbf{R}; \hat{\mathbf{k}}, E) | \vec{\epsilon} \cdot \vec{\mu} | \psi_i \rangle|^2 \quad (1)$$

where $\sum_{vjm_j}$ represents a summation over all possible final states of the system with energy E scattered into the direction $\hat{\mathbf{k}}$, $\vec{\mu}$ is the transition dipole moment, $\vec{\epsilon}$ is the electric field vector of the photodissociating light, $\psi^-_{vjm_j}(\mathbf{r}, \mathbf{R}; \hat{\mathbf{k}}, E)$ is a continuum scattering wavefunction with well defined outgoing internal fragment states and ψ_i is the initial bound state wavefunction.

We can now rearrange this equation by expanding out the squared matrix element and bringing the summation into the centre of the expression.

$$\begin{aligned}\sigma_{tot}(E) &= \frac{2\pi^2 v}{c\epsilon_0} \sum_{vjm_j} \int \mathrm{d}\hat{\mathbf{k}} \langle \psi_i | \vec{\epsilon} \cdot \vec{\mu} | \psi^-_{vjm_j}(\mathbf{r}, \mathbf{R}; \hat{\mathbf{k}}, E) \rangle \\ &\quad \times \langle \psi^-_{vjm_j}(\mathbf{r}, \mathbf{R}; \hat{\mathbf{k}}, E) | \vec{\epsilon} \cdot \vec{\mu} | \psi_i \rangle \\ &= \frac{2\pi^2 v}{c\epsilon_0} \langle \psi_i | \vec{\epsilon} \cdot \vec{\mu} | \Big\{ \sum_{vjm_j} \int \mathrm{d}\hat{\mathbf{k}} | \psi^-_{vjm_j}(\mathbf{r}, \mathbf{R}; \hat{\mathbf{k}}, E) \rangle \\ &\quad \times \langle \psi^-_{vjm_j}(\mathbf{r}, \mathbf{R}; \hat{\mathbf{k}}, E) | \Big\} | \vec{\epsilon} \cdot \vec{\mu} | \psi_i \rangle \end{aligned} \quad (2)$$

The curly bracket in the middle of Eq. (2) is a projection operator onto a wavefunction of energy E with a summation over all other quantum numbers. It is therefore an identity operator, but with a projection onto a well defined total energy. An alternative way of writing this is:

$$\begin{aligned}&\sum_{vjm_j} \int \mathrm{d}\hat{\mathbf{k}} | \psi^-_{vjm_j}(\mathbf{r}, \mathbf{R}; \hat{\mathbf{k}}, E) \rangle \langle \psi^-_{vjm_j}(\mathbf{r}, \mathbf{R}; \hat{\mathbf{k}}, E) | \\ &\quad = \delta(\hat{\mathbf{H}} - E) \hat{\mathbf{I}} \end{aligned} \quad (3)$$

The Dirac delta function of the energy, $\delta(\hat{\mathbf{H}} - E)$, can be written as a Fourier transform over time:

$$\delta(\hat{\mathbf{H}} - E) = \frac{1}{2\pi\hbar} \int_{-\infty}^{\infty} \mathrm{d}t \exp\left[\frac{-i(\hat{\mathbf{H}} - E)t}{\hbar}\right]. \quad (4)$$

This expression contains within it the time-evolution operator, $\exp\left[\frac{-i\hat{\mathbf{H}}t}{\hbar}\right]$, and is the key to introducing the time variable into the calculation of the photodissociation cross section. We now define the product of the initial wavefunction and the transition dipole moment as the initial wavepacket, $\Phi_i(\mathbf{r}, \mathbf{R}, t = 0)$:

$$|\Phi(\mathbf{r}, \mathbf{R}, t = 0)\rangle = \vec{\epsilon} \cdot \vec{\mu} |\psi_i\rangle, \quad (5)$$

where $\vec{\epsilon}$ is the unit length electric field vector of the light wave.

The action of the time-evolution operator on the initial wavepacket (Eq. 5) gives a time evolved wavepacket at time t:

$$|\Phi(\mathbf{r}, \mathbf{R}, t)\rangle = \exp\left[\frac{-i\hat{\mathbf{H}}t}{\hbar}\right] \Phi(\mathbf{r}, \mathbf{R}, t = 0), \quad (6)$$

Using Eqs. (3–6) in Eq. (2) we get the following expression for the total integral photodissociation cross section:

$$\begin{aligned}\sigma_{\mathrm{tot}}(E) &= \frac{\pi v}{c\epsilon_0 \hbar} \int_{-\infty}^{\infty} \mathrm{d}t \exp\left[\frac{iEt}{\hbar}\right] \langle \Phi(\mathbf{r}, \mathbf{R}, t = 0) | \Phi(\mathbf{r}, \mathbf{R}, t) \rangle \\ &= \frac{2\pi v}{c\epsilon_0 \hbar} \int_{0}^{\infty} \mathrm{d}t \exp\left[\frac{iEt}{\hbar}\right] \langle \Phi(\mathbf{r}, \mathbf{R}, t = 0) | \Phi(\mathbf{r}, \mathbf{R}, t) \rangle. \end{aligned} \quad (7)$$

The term $\langle \Phi(\mathbf{r}, \mathbf{R}, t = 0) | \Phi(\mathbf{r}, \mathbf{R}, t) \rangle$ is a so-called autocorrelation function involving the overlap of an initial wavepacket with the wavepacket evolved to a later time. The total cross section is then a Fourier transform of this time-dependent function at a particular energy. The Fourier transform converts the time-dependent quantity to the energy-dependent quantity of interest.

For partial and differential photodissociation cross sections corresponding derivations and analyses are given in Refs. [36, 45]. The derivation of time-dependent expressions for reactive scattering cross sections and **S** matrices is discussed in Refs. [36, 46, 47].

3 The Real Wavepacket method

The so-called time-independent wavepacket method for reactive scattering was developed by Kouri and co-workers [48–55]. The method is based on the time-dependent formalism combined with the Chebyshev expansion of the time-evolution operator [30−32]. Then, instead of performing the time-evolution of the wavepacket, the formal equations for the evaluation of the **S** matrix, including the Chebyshev expansion of the evolution operator, are written down. The summation over the Chebyshev polynomial orders and the integration over time are exchanged, and the integration over time is performed [41]. The result is a formalism for the evaluation of the scattering **S** matrix involving a summation over different orders of the Chebyshev polynomials with the coefficients in the expansion being computed iteratively by repeated operation on the (time-independent) wavepacket with a scaled Hamiltonian operator.

Gray and the present author developed a similar procedure, called the Real Wavepacket method, for computing reactive scattering probabilities, but starting from a completely different viewpoint [56]. Their starting point was an iterative equivalent to the time-dependent Schrödinger equation.

The time-dependent Schrödinger equation is:

$$i\hbar\frac{\partial\Phi(t)}{\partial t} = \hat{\mathbf{H}}\Phi(t) \tag{8}$$

If the Hamiltonian, $\hat{\mathbf{H}}$, does not depend on time, this equation has the analytic solution:

$$\Phi(t) = \exp\left[\frac{-i\hat{\mathbf{H}}t}{\hbar}\right]\Phi(t=0). \tag{9}$$

$\exp\left[\frac{-i\hat{\mathbf{H}}\tau}{\hbar}\right]$ is the time-evolution operator and propagates the wavepacket forward in time from $t = 0$ to $t = \tau$. Expanding the propagator in terms of cosines and sines, we may write:

$$\Phi(t+\tau) = \cos\left[\frac{\hat{\mathbf{H}}\tau}{\hbar}\right]\Phi(t) - i\sin\left[\frac{\hat{\mathbf{H}}\tau}{\hbar}\right]\Phi(t). \tag{10}$$

The corresponding expression for the backward propagation, from t to $t - \tau$ is:

$$\Phi(t-\tau) = \cos\left[\frac{\hat{\mathbf{H}}\tau}{\hbar}\right]\Phi(t) + i\sin\left[\frac{\hat{\mathbf{H}}\tau}{\hbar}\right]\Phi(t). \tag{11}$$

By adding Eqs. (10) and (11) we obtain [57]:

$$\Phi(t+\tau) = 2\cos\left[\frac{\hat{\mathbf{H}}\tau}{\hbar}\right]\Phi(t) - \Phi(t-\tau). \tag{12}$$

This equation is exact and constitutes an iterative equation equivalent to the time-dependent Schrödinger equation [57–59]. The iterative process itself does not involve the imaginary number i and therefore, if $\Phi(t)$ and $\Phi(t-\tau)$ were the real parts of the wavepacket, then $\Phi(t+\tau)$ would also be real and would be the real part of the exact wavepacket at time $(t+\tau)$. Thus the real part of a complex wavepacket can be propagated forward in time without reference to the imaginary part. This is the basis of the Real Wavepacket method.

The iterative procedure of Eq. (12) involves the evaluation of the cosine of $\hat{\mathbf{H}}$ acting on a wavepacket. This is a difficult operation to perform. In the Real Wavepacket method a mapping of the Hamiltonian operator is performed to overcome this problem.

$$f(\hat{\mathbf{H}}_s) = -\frac{\hbar}{\tau}\cos^{-1}(\hat{\mathbf{H}}_s). \tag{13}$$

where $\hat{\mathbf{H}}_s$ is a shifted and scaled Hamiltonian. This shifting and scaling is required so as to make the mapping single valued and is such as to make the range of the Hamiltonian operator lie in the interval $-1 \le \hat{\mathbf{H}}_s \le 1$;

$$\hat{\mathbf{H}}_s = \frac{\hat{\mathbf{H}} - \hat{\mathbf{I}}\left(\frac{\Delta E}{2} + V_{\min}\right)}{\frac{\Delta E}{2}} \tag{14}$$

where we have replaced $E_{\min}$, the minimum energy, by $V_{\min}$. As $V_{\min} \le E_{\min}$ this is always permissible and just leads to a slight overestimate of the range of the Hamiltonian operator. Note that this scaling and shifting of the spectrum is identical to that required for the use of the Chebyshev expansion of the time-evolution operator [30, 34, 41].

The use of this mapping (Eq. 13) means that we are no longer solving the time-dependent Schrödinger equation, but rather a modified equation of the form:

$$i\hbar\frac{\partial\Phi_f(t)}{\partial t} = f(\hat{\mathbf{H}}_s)\Phi_f(t), \tag{15}$$

where a subscript "f" has been placed on the wavefunction to emphasise that it is the solution of a mapped equation rather than of the original time-dependent Schrödinger equation. The same arguments which led to the iterative equation equivalent to the time-dependent Schrödinger equation Eq. (5), now lead to the simplified form:

$$\Phi_f^R(t+\tau) = 2\hat{\mathbf{H}}_s\Phi_f^R(t) - \Phi_f^R(t-\tau). \tag{16}$$

where the superscript R in $\Phi_f^R(t)$ indicates that only the real part of the wavepacket is used.

I emphasise again that this equation is exact and is completely equivalent to the time-dependent Schrödinger equation.

Gray [57] has shown that, when an absorbing technique is included in the propagation of the wavepacket to prevent it from reaching the edge of a finite grid, the absorption

should be performed in the same way as was later discussed by Mandelstam and Taylor [60] namely:

$$\Phi_f^R(t+\tau) = \hat{\mathbf{A}}\left\{2\hat{\mathbf{H}}_s\Phi_f^R(t) - \hat{\mathbf{A}}\Phi_f^R(t-\tau)\right\} \tag{17}$$

where $\hat{\mathbf{A}}$ is a damping operator and may have the form $\exp[-V_{\text{abs}}(x)\tau/\hbar]$, such that $V_{\text{abs}}(r)$ is non-zero only in an absorbing region close to the edge of the grid and is in general similar in form to the negative imaginary part of the more widely used negative imaginary absorbing potentials [61, 62].

Note that the time step, τ, has been included in the mapping of the Hamiltonian operator (Eq. 13). In practise all the Fourier transforms over time (see Eq. 7) are performed using a trapezoid rule approach. With this in mind we can now replace the integrations over time by summations over the iteration number. Therefore, we replace time using $t = k\tau$, where k is the iteration number and τ is the time step.

$$\begin{aligned}\sigma_{\text{tot}}(E) &= \frac{2\pi v}{c\epsilon_0\hbar}\int_0^\infty \mathrm{d}t\,\exp\left[\frac{iEt}{\hbar}\right]\langle\Phi(\mathbf{r},\mathbf{R},t=0)|\Phi(\mathbf{r},\mathbf{R},t)\rangle \\ &= \frac{2\pi v}{c\epsilon_0\hbar}\sum_{k=0}^{k=\infty}\tau\,\exp\left[\frac{iEk\tau}{\hbar}\right]\langle\Phi_0|\Phi_k\rangle \end{aligned}\tag{18}$$

where $\Phi_k = \Phi(\mathbf{r},\mathbf{R},k\tau)$.

We now use the mapping $E_s \rightarrow f$ (E_s) as in Eq. (13) (also $\Phi_k \rightarrow \Phi_{f,k}$, see Eq. (15)) and obtain:

$$\sigma_{\text{tot}}(f) = \frac{\mathrm{d}f}{\mathrm{d}E}\frac{2\pi v}{c\epsilon_0}\sum_{k=0}^{k=\infty}\frac{\tau}{\hbar}\exp\left[\frac{ifk\tau}{\hbar}\right]\left\langle\Phi_{f,0}|\Phi_{f,k}\right\rangle. \tag{19}$$

The factor $\frac{\mathrm{d}f}{\mathrm{d}E}$ which has been introduced into Eq. (19) arises from the conversion of the Dirac delta function in Eq. (3) from a function of E to a function of f [41, 56]. In Ref. [41] it is shown that:

$$\frac{\mathrm{d}f}{\mathrm{d}E} = \frac{\hbar}{\tau}\frac{1}{\sqrt{1-E_s^2}}\frac{2}{\Delta E} \tag{20}$$

There remains a factor of τ in the exponential in Eq. (19). The arbitrary value of the time interval τ cannot change any measurable quantity. We therefore choose to set $\frac{\tau}{\hbar} = 1$. This procedure is in keeping with past derivations and results in agreement with expressions for quantities such as the scattering $\mathbf{S}$ matrix derived using different methods [48]. Making this change and substituting Eq. (20) into Eq. (19) we obtain:

$$\sigma_{\text{tot}}(f) = \frac{4\pi v}{c\epsilon_0\Delta E}\frac{1}{\sqrt{1-E_s^2}}\sum_{k=0}^{k=\infty}\exp[ifk]\left\langle\Phi_{f,0}|\Phi_{f,k}\right\rangle. \tag{21}$$

As it stands the iterated wavepackets, $\Phi_{f,k}$ are complex. In Ref. [56] and in "Appendix F" of Ref. [41] we show that if only the real part of the wavepacket is used, the resulting cross section (or matrix element) must be multiplied by a factor or 2. Our final expression for the total integral photodissociation cross section therefore becomes:

$$\sigma_{\text{tot}}(f) = \frac{8\pi v}{c\epsilon_0\Delta E}\frac{1}{\sqrt{1-E_s^2}}\sum_{k=0}^{k=\infty}\exp[ifk]\left\langle\Phi_{f,0}|\Phi_{f,k}^R\right\rangle. \tag{22}$$

where $\Phi_{f,k}^R$ indicates the real part of the wavepacket. No superscript R has been placed on the initial wavepacket $\Phi_{f,0}$ as it is in any case real.

There is a small residual difficulty in the determination of the first iterate $\Phi_{f,1}$. This is a complex wavepacket and cannot be determined using the iteration method of Eq. (16) as only a single previous iterate is known. We therefore need to determine it using Eq. (10) or its equivalent [see Ref. 56]:

$$\begin{aligned}\Phi_{f,1} &= \cos\left[\frac{f(\hat{\mathbf{H}}_s)\tau}{\hbar}\right]\Phi_0 - i\sin\left[\frac{f(\hat{\mathbf{H}}_s)\tau}{\hbar}\right]\Phi_0 \\ &= \cos\left[\frac{-\frac{\hbar}{\tau}\cos^{-1}(\hat{\mathbf{H}}_s)\tau}{\hbar}\right]\Phi_0 - i\sin\left[\frac{-\frac{\hbar}{\tau}\cos^{-1}(\hat{\mathbf{H}}_s)\tau}{\hbar}\right]\Phi_0 \\ &= \cos\left[-\cos^{-1}(\hat{\mathbf{H}}_s)\right]\Phi_0 - i\sin\left[-\cos^{-1}(\hat{\mathbf{H}}_s)\right]\Phi_0 \\ &= \hat{\mathbf{H}}_s\Phi_0 + i\sin\left[\cos^{-1}(\hat{\mathbf{H}}_s)\right]\Phi_0 \\ &= \hat{\mathbf{H}}_s\Phi_0 + i\sqrt{1-\left(\cos\left[\cos^{-1}(\hat{\mathbf{H}}_s)\right]\right)^2}\Phi_0 \\ &= \hat{\mathbf{H}}_s\Phi_0 + i\sqrt{1-\left(\hat{\mathbf{H}}_s\right)^2}\Phi_0. \end{aligned}\tag{23}$$

The evaluation of $\sqrt{1-\left(\hat{\mathbf{H}}_s\right)^2}\Phi_0$ is discussed in detail in "Appendix C" of Ref. [41]. Once $\Phi_{f,1}$ has been evaluated, we take its real part to obtain $\Phi_{f,1}^R = \mathcal{R}]\{\Phi_{f,1}\}$ and further iterates are obtained using the recursive relationship (see Eq. 16):

$$\Phi_{f,k}^R = 2\hat{\mathbf{H}}_s\Phi_{f,k-1}^R - \Phi_{f,k-2}^R. \tag{24}$$

The advantages of using only the real part of the wavepacket accrue in terms of both storage and a large reduction in the number of arithmetic operations required for the propagation of the wavepacket. An advantage of using a summation over the iterate number, rather than using a Chebyshev expansion of the time-evolution operator to repeatedly propagate the wavepacket forward by a small increment of time, is that overall a far fewer number of operations of the Hamiltonian operator are required.

I have outlined above the application of the Real Wavepacket method to the evaluation of the total integral photodissociation cross section. Its application to other types of photodissociation and reactive scattering cross section are described in Ref. [41] and elsewhere. This reference also gives comparisons with other related methods [48–70].

4 Final state analysis

4.1 Time-independent formulation

In both photodissociation and reactive scattering we often seek information about the final product quantum states. This information takes the form of partial cross sections. The cross sections may be either differential (scattering angle dependent) partial cross sections or integral partial cross sections, which provide the total probability of producing products in specified quantum states. In either case the final state of the scattered products must be analysed. There are four somewhat different ways of performing this analysis. The first method of analysis involves computing the energy-dependent wavepacket and overlapping it with a test Gaussian-like function in the product scattering coordinate multiplied by a wavefunction for a pure quantum state of the products [52, 71, 72–75]. This gives an amplitude for forming a particular product quantum state from a well specified initial quantum state of the original molecule or reactants. The other methods involve examining the time-dependent wavepacket in the exit channel of the reaction or photodissociation process. In the first of these the time-dependent wavepacket is projected onto product quantum states in the exit channel and is analysed into its component radial wave vector components, thus defining the scattering into a given final product quantum state and total energy [76]. This is very similar to the first method, but does not involve specific transformation from the time to energy domains. The third method involves projecting the wavepacket in the exit channel onto specific product quantum states and then calculating the flux of each of the states through a surface placed perpendicular to the outgoing scattering coordinate [77, 78]. The final method, which is the one we will concentrate on, involves taking a cut through the time-dependent wavepacket at a fixed, large, value of the scattering coordinate at each time step. This cut through the wavepacket is then projected onto the different product quantum states of the system yielding a time-dependent coefficient for each product quantum state. The Fourier transform of these coefficients then yield energy-dependent amplitudes for the production of each of the possible product quantum states. These amplitudes may then be used to compute either S matrix elements or state-specific reaction probabilities [45, 47, 79].

The equation for the integral partial photodissociation cross section may be written in the form (see Eq. 1):

$$\sigma_{vjm_j}(E) = \frac{2\pi^2 \nu}{c\epsilon_0} \int d\hat{\mathbf{k}} |\langle \psi^-_{vjm_j}(\mathbf{r}, \mathbf{R}; \hat{\mathbf{k}}, E) | \vec{\epsilon} \cdot \vec{\mu} | \psi_i \rangle|^2 \qquad (25)$$

We now need to express the continuum wavefunction $\psi^-_{vjm_j}(\mathbf{r}, \mathbf{R}; \hat{\mathbf{k}}, E)$ and the initial wavepacket, "$\vec{\epsilon} \cdot \vec{\mu} | \psi_i \rangle$" (see Eq. 5), in terms of body-fixed coordinates and to utilise the fact that functions belonging to different total angular momenta are mutually orthogonal.

The continuum wavefunction can be written in the form [36]:

$$\begin{aligned} \psi^-_{vjm_j}(\mathbf{r}, \mathbf{R}; \hat{\mathbf{k}}, E) = & \sum_{JM} \sum_{lm_l p} Y^*_{lm_l}(\hat{\mathbf{k}}) (jlJM | jm_j lm_l) \\ & \times \sum_{K=\lambda}^{J} (Jjl0 | JKj - K) \\ & \times \sum_{K'=\lambda}^{J} \Phi^{-JvjKp}_{K'}(r, R, \theta; E) | J, K', M, p > , \end{aligned} \qquad (26)$$

where

$$\begin{aligned} \Phi^{-JvjKp}_{K'}(r, R, \theta; E) = & \left(\frac{\mu k_{vj}}{\hbar^2 (2\pi)^3} \right)^{\frac{1}{2}} 4\pi \sum_{v'j'} \left\{ \frac{2(-1)^{j-K}}{\sqrt{2(1+\delta_{0,K})}} \right\} \\ & \times \frac{\Phi^{(JvjKp)}_{v'j'K'}(R)}{R} \Theta_{j'K'}(\theta) \chi_{v'j'}(r). \end{aligned} \qquad (27)$$

and $|J, K, M, p\rangle$ are parity adapted eigenfunctions [80] for the overall rotation of the system corresponding to a total angular momentum (J) and to specified space-fixed (M) and body-fixed (K) z components; $\Phi^{-JvjKp}(r, R, \theta; E)$ is a body-fixed wavefunction with the correct boundary conditions [36, 81] so as to yield the asymptotic behaviour of a pure outgoing plane wave, $(J\, j\, l\, 0 \mid J\, K\, j - K)$ are Clebsch–Gordan angular momentum coupling coefficients, [82, 83] r, R, θ are the body-fixed Jacobi coordinates with θ being the angle between the scattering coordinate $\mathbf{R}$ and the diatomic molecular axis direction, $\mathbf{r}$ [see Ref. 80] and $\Theta_{j'K'}(\theta)$ are normalised associated Legendre Polynomials [83].

The parity adapted total angular momentum eigenfunctions [80–83] are composed of the sum or difference of two Wigner D matrices and are functions of the three Euler angles which orient the three atoms in the laboratory frame.

The asymptotic form of the body-fixed radial scattering wavefunction, $\Phi^{(JvjK)}_{v'j'K'}(R)$, is [81, 84]:

$$\begin{aligned} \Phi^{(JvjK)}_{v'j'K'}(R) \quad \widetilde{R \to \infty} & \frac{1}{2ik_{vj}} \Bigg[e^{ik_{v'j'}R} \delta_{vv'} \delta_{jj'} \delta_{KK'} \\ & - S^{Jp*}_{vjK, v'j'K'} \left(\frac{k_{v'j'}}{k_{vj}} \right)^{\frac{1}{2}} e^{-ik_{v'j'}R} \Bigg] \end{aligned} \qquad (28)$$

The initial wavefunction, ψ_i, appearing in Eq. (1) is also an eigenfunction of the total angular momentum, with $J = J_i$, of its space-fixed z component, $M = M_i$, and of the parity, $(-1)^{J+K+p}$. It may be written in the form:

$$\psi_i \equiv \Psi^{J_i,M_i,p}(r,R,\theta,\omega) = \sum_{K_i=\lambda}^{J_i} \psi^{J_i,K_i,p}(r,R,\theta)|J_i,K_i,M_i,p\rangle \tag{29}$$

where ω represents the Euler angles which orient the molecule in the laboratory reference frame.

The initial wavepacket for the photodissociation process, as given in Eq. (5), is $\Phi(\mathbf{r},\mathbf{R},t=0) = \vec{\epsilon}\cdot\vec{\mu}|\psi_i\rangle$. When written in terms of the parity adapted eigenfunctions of total J, this can be shown to be equal to [80]:

$$\begin{aligned}\Phi_i(\mathbf{r},\mathbf{R},t=0) &= \vec{\epsilon}\cdot\vec{\mu}|\psi_i\rangle \\ &= \sum_{J'=J_i-1}^{J_i+1}(-1)^{m+M_i}\begin{pmatrix}1 & J_i & J'\\ m & M_i & -(m+M_i)\end{pmatrix} \\ &\times\left\{\sum_{K=\lambda'}^{J'}\Phi_i^{J'K}(r,R,\theta,t=0)|J',K,M_i+m,p'\rangle\right\}\end{aligned} \tag{30}$$

where the detailed form of $\Phi_i^{J'K}(r,R,\theta,t=0)$ is given in "Appendix A" [80, 85].

As expected from the vector property of the polarisation vector of the incident light beam the initial wavepacket becomes a linear combination of functions with up to three possible values of the total angular momentum, differing from J_i by at most one.

The label m relates to the nature of the space-fixed electric field polarisation vector. $m=0$ denotes linearly polarised light with the electric field vector pointing along the space-fixed z axis, while $m=\pm1$ corresponds to circularly polarised light, with the space-fixed z axis pointing along the propagation direction of the light beam. The parity factor, $(-1)^{p'}$, of the wavefunction for nuclear motion is the same as that of the initial wavefunction if the electronic transition is perpendicular, i.e. the transition dipole moment is perpendicular to the molecular plane, and it is opposite to the initial parity for a parallel electronic transition.

Substituting Eqs. (26) and (30) into Eq. (25) we obtain:

$$\begin{aligned}\sigma_{vjm_j}(E) &= \frac{2\pi^2 v}{c\epsilon_0}\int d\hat{\mathbf{k}}\left|\left\langle\sum_{JM}\sum_{lm_lp}Y^*_{lm_l}(\hat{\mathbf{k}})(jlJM|jm_jlm_l)\right.\right. \\ &\times\sum_{K=\lambda}^{J}(Jjl0|JKj-K) \\ &\times\sum_{K'=\lambda}^{J}\Phi_{K'}^{-JvjKp}(r,R,\theta;E)\langle J,K',M,p| \\ &\times\sum_{J'=J_i-1}^{J_i+1}(-1)^{m+M_i}\begin{pmatrix}1 & J_i & J'\\ m & M_i & -(m+M_i)\end{pmatrix} \\ &\times\left.\left\{\sum_{K''=\lambda'}^{J'}\Phi_i^{J'K''}(r,R,\theta,t=0)\right\rangle|J',K'',M_i+m,p'\rangle\right\}\Bigg|^2 \\ &= \frac{2\pi^2 v}{c\epsilon_0}\int d\hat{\mathbf{k}}\left|\sum_{JM}\sum_{lm_lp}Y^*_{lm_l}(\hat{\mathbf{k}})(jlJM|jm_jlm_l)\right. \\ &\times\sum_{K=\lambda}^{J}(Jjl0|JKj-K) \\ &\times\sum_{K'=\lambda}^{J}\sum_{J'=J_i-1}^{J_i+1}(-1)^{m+M_i}\begin{pmatrix}1 & J_i & J'\\ m & M_i & -(m+M_i)\end{pmatrix} \\ &\times\left\{\sum_{K''=\lambda'}^{J'}\left\langle\Phi_{K'}^{-JvjKp}(r,R,\theta;E)|\Phi_i^{J'K''}(r,R,\theta,t=0)\right\rangle\right. \\ &\times\left.\left.\delta_{J,J'}\delta_{K',K''}\delta_{M,(M_i+m)}\delta_{p,p'}\right\}\right|^2 \\ &= \frac{2\pi^2 v}{c\epsilon_0}\int d\hat{\mathbf{k}}\left|(-1)^{m+M_i}\sum_{J=J_i-1}^{J_i+1}\sum_{lm_l}Y^*_{lm_l}(\hat{\mathbf{k}})\right. \\ &\times(jlJ(M_i+m)|jm_jlm_l)\sum_{K=\lambda}^{J}(Jjl0|JKj-K) \\ &\times\begin{pmatrix}1 & J_i & J\\ m & M_i & -(m+M_i)\end{pmatrix} \\ &\times\left.\sum_{K'=\lambda}^{J}\left\langle\Phi_{K'}^{-JvjKp}(r,R,\theta;E)|\Phi_i^{JK'}(r,R,\theta,t=0)\right\rangle\right|^2\end{aligned} \tag{31}$$

where $p=p_i$ for a perpendicular transition and $p=(p_i+1)$ for a parallel transition.

We now define the photofragmentation $\mathbf{T}$ matrix element as:

$$T_{vj}^{JKp} = \sum_{K'=\lambda}^{J}\langle\Phi_{K'}^{-JvjKp}(r,R,\theta;E)|\Phi_i^{JK'}(r,R,\theta,t=0)\rangle. \tag{32}$$

Using this definition in Eq. (31) we obtain:

$$\begin{aligned}\sigma_{vjm_j}(E) &= \frac{2\pi^2 v}{c\epsilon_0}\int d\hat{\mathbf{k}}\left|(-1)^{m+M_i}\sum_{J=J_i-1}^{J_i+1}\sum_{lm_l}Y^*_{lm_l}(\hat{\mathbf{k}})\right. \\ &\times(jlJ(M_i+m)|jm_jlm_l)\sum_{K=\lambda}^{J}(Jjl0|JKj-K) \\ &\times\left.\begin{pmatrix}1 & J_i & J\\ m & M_i & -(m+M_i)\end{pmatrix}T_{vj}^{JKp}\right|^2\end{aligned} \tag{33}$$

We now expand out the squared quantity and then perform the integration over the scattering angles $\hat{\mathbf{k}}$.

$$\sigma_{vjm_j}(E) = \frac{2\pi^2 v}{c\epsilon_0}\Bigg\{ \sum_{J=J_i-1}^{J_i+1} \sum_{lm_l} \sum_{J'=J_i-1}^{J_i+1} \sum_{l'm'_l} \times \left\{ \int d\hat{\mathbf{k}} Y^*_{lm_l}(\hat{\mathbf{k}}) Y_{l'm'_l}(\hat{\mathbf{k}}) \right\} (jlJ(M_i+m)|jm_j lm_l) \times (jl'J'(M_i+m)|jm_j lm'_l) \sum_{K=\lambda}^{J} \sum_{K'=\lambda}^{J'} (Jjl0|JKj-K) \times (J'jl'0|J'K'j-K') \begin{pmatrix} 1 & J_i & J \\ m & M_i & -(m+M_i) \end{pmatrix} \times \begin{pmatrix} 1 & J_i & J' \\ m & M_i & -(m+M_i) \end{pmatrix} T^{JKp}_{vj} T^{J'Kp*}_{vj} \Bigg\}$$

$$= \frac{2\pi^2 v}{c\epsilon_0}\Bigg\{ \sum_{J=J_i-1}^{J_i+1} \sum_{lm_l} \sum_{J'=J_i-1}^{J_i+1} \times \sum_{l'm'_l} \delta_{l,l'} \delta_{m_l,m'_l} (jlJ(M_i+m)|jm_j lm_l) \times (jl'J'(M_i+m)|jm_j l'm'_l) \sum_{K=\lambda}^{J} \sum_{K'=\lambda}^{J'} (Jjl0|JKj-K) \times (J'jl'0|J'K'j-K') \begin{pmatrix} 1 & J_i & J \\ m & M_i & -(m+M_i) \end{pmatrix} \times \begin{pmatrix} 1 & J_i & J' \\ m & M_i & -(m+M_i) \end{pmatrix} T^{JKp}_{vj} T^{J'Kp*}_{vj} \Bigg\}$$

$$= \frac{2\pi^2 v}{c\epsilon_0}\Bigg\{ \sum_{J=J_i-1}^{J_i+1} \sum_{lm_l} \sum_{J'=J_i-1}^{J_i+1} (jlJ(M_i+m)|jm_j lm_l) \times (jlJ'(M_i+m)|jm_j lm_l) \sum_{K=\lambda}^{J} \sum_{K'=\lambda}^{J'} (Jjl0|JKj-K)(J'jl0|J'K'j-K') \times \begin{pmatrix} 1 & J_i & J \\ m & M_i & -(m+M_i) \end{pmatrix} \begin{pmatrix} 1 & J_i & J' \\ m & M_i & -(m+M_i) \end{pmatrix} \times T^{JKp}_{vj} T^{J'K'p*}_{vj} \Bigg\} \tag{34}$$

This is the equation for the integral partial cross section for producing a diatomic fragment in the quantum state vjm_j from a triatomic molecule in the state J_i M_i. To my knowledge this is the first time this cross section has been formulated in this manner. Note that because J_i, M_i, j and m_j are known, the range of the summations over l and m_l are quite limited and may be easily performed.

If we now sum over all possible fragment m_j quantum numbers we obtain:

$$\sigma_{vj}(E) = \frac{2\pi^2 v}{c\epsilon_0}\Bigg\{ \sum_{J=J_i-1}^{J_i+1} \sum_{l} \sum_{J'=J_i-1}^{J_i+1} \Bigg[\sum_{m_l m_j} (jlJ(M_i+m)|jm_j lm_l) \times (jlJ'(M_i+m)|jm_j lm_l) \Bigg] \sum_{K=\lambda}^{J} \sum_{K'=\lambda}^{J'} (Jjl0|JKj-K)(J'jl0|J'K'j-K') \times \begin{pmatrix} 1 & J_i & J \\ m & M_i & -(m+M_i) \end{pmatrix} \times \begin{pmatrix} 1 & J_i & J' \\ m & M_i & -(m+M_i) \end{pmatrix} T^{JKp}_{vj} T^{J'K'p*}_{vj} \Bigg\} \tag{35}$$

Now using the orthogonality relationship of the Clebsch–Gordan coefficients (see Eq. 2.8 of Ref. [83]) to simplify the square bracket in the first line of Eq. (35) we obtain:

$$\sigma_{vj}(E) = \frac{2\pi^2 v}{c\epsilon_0}\Bigg\{ \sum_{J=J_i-1}^{J_i+1} \sum_{l} \sum_{J'=J_i-1}^{J_i+1} \delta_{J,J'} \sum_{K=\lambda}^{J} \sum_{K'=\lambda}^{J'} (Jjl0|JKj-K) \times (J'jl0|J'K'j-K') \begin{pmatrix} 1 & J_i & J \\ m & M_i & -(m+M_i) \end{pmatrix} \times \begin{pmatrix} 1 & J_i & J' \\ m & M_i & -(m+M_i) \end{pmatrix} T^{JKp}_{vj} T^{J'K'p*}_{vj} \Bigg\}$$

$$= \frac{2\pi^2 v}{c\epsilon_0}\Bigg\{ \sum_{J=J_i-1}^{J_i+1} \sum_{K=\lambda}^{J} \sum_{K'=\lambda}^{J} \times \left\{ \sum_{l} (Jjl0|JKj-K)(Jjl0|JK'j-K') \right\} \times \begin{pmatrix} 1 & J_i & J \\ m & M_i & -(m+M_i) \end{pmatrix} \begin{pmatrix} 1 & J_i & J \\ m & M_i & -(m+M_i) \end{pmatrix} \times T^{JKp}_{vj} T^{JK'p*}_{vj} \Bigg\}$$

$$= \frac{2\pi^2 v}{c\epsilon_0}\Bigg\{ \sum_{J=J_i-1}^{J_i+1} \sum_{K=\lambda}^{J} \sum_{K'=\lambda}^{J} \delta_{K,K'} \begin{pmatrix} 1 & J_i & J \\ m & M_i & -(m+M_i) \end{pmatrix} \times \begin{pmatrix} 1 & J_i & J \\ m & M_i & -(m+M_i) \end{pmatrix} T^{JKp}_{vj} T^{JK'p*}_{vj} \Bigg\}$$

$$= \frac{2\pi^2 v}{c\epsilon_0}\Bigg\{ \sum_{J=J_i-1}^{J_i+1} \sum_{K=\lambda}^{J} \begin{pmatrix} 1 & J_i & J \\ m & M_i & -(m+M_i) \end{pmatrix} \times \begin{pmatrix} 1 & J_i & J \\ m & M_i & -(m+M_i) \end{pmatrix} T^{JKp}_{vj} T^{JKp*}_{vj} \Bigg\} \tag{36}$$

where I have used the orthogonality relationship of the 3j symbols (see Eq. 2.33 of Ref. [83]) in the above manipulations.

Eq. (36) may alternatively be expressed in the form:

$$\sigma_{vj}(E) = \frac{2\pi^2 v}{c\epsilon_0} \sum_{J=J_i-1}^{J_i+1} \sum_{K=\lambda}^{J} \left| \begin{pmatrix} 1 & J_i & J \\ m & M_i & -(m+M_i) \end{pmatrix} T^{JKp}_{vj} \right|^2 \tag{37}$$

Equation (37) is the expression for the integral partial cross section for the production of diatomic fragments in quantum state vj summed over all the m_j states, arising from state J_i, M_i of the initial triatomic molecule. If we average over the initial M_i states [81] of the triatomic and use the orthogonality and symmetry relationships of the 3j symbols (see Eqs. 2.29 and 2.32 of Ref. [83]) we obtain:

$$\bar{\sigma}_{vj}(E) = \frac{1}{2J_i+1}\sum_{M_i}\sigma_{vj}(E) = \frac{2\pi^2 v}{3c\epsilon_0}\frac{1}{2J_i+1}\sum_{J=J_i-1}^{J_i+1}\sum_{K=\lambda}^{J}\left|T_{vj}^{JKp}\right|^2. \tag{38}$$

4.2 Time-dependent formulation

The above derivation was made entirely within a time-independent framework. The photofragmentation **T** matrix elements encompass all the dynamics of the photodissociation process. The evaluation of these **T** matrix elements using a time-dependent wavepacket approach has been outlined in "Appendix C" of Ref. [36]. As mentioned above the key to the calculation is the definition of an analysis line. This analysis line is drawn in the asymptotic region of the potential energy surface and is defined by a constant value of the scattering coordinate, $R = R_\infty$. An illustration of such an analysis line is given in Fig. 1.

The function of the analysis line is that we take a cut through the wavepacket at each time step (or at each iteration), and we then project the function obtained in this way onto the asymptotic product fragment wavefunctions, thus obtaining the time-dependent coefficients $C_{vj}^{JK}(t)$.

$$C_{vj}^{JK}(t) = \left\langle \Theta_{jK}(\theta)\chi_{vj}(r)\middle|\Phi_i^{JK}(r, R=R_\infty, \theta, t)\right\rangle \tag{39}$$

The half Fourier transform over time of this coefficient then yields an energy-dependent amplitude, $A_{vj}^{JK}(E)$.

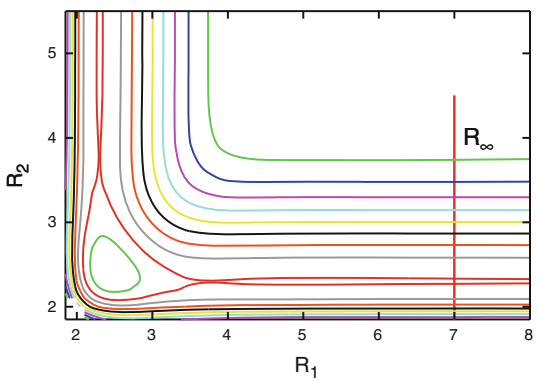

Fig. 1 Illustration of an analysis line in the asymptotic region of the ground electronic state of ozone molecule (O_2–O)

$$A_{vj}^{JK}(E) = \frac{1}{2\pi}\int_{t=0}^{\infty}\exp(iEt/\hbar)C_{vj}^{JK}(t)\mathrm{d}t \tag{40}$$

The photofragmentation **T** matrix elements are then obtained from these amplitudes using the relationship:

$$T_{vj}^{JKp} = i(-1)^{K-j}A_{vj}^{JK}(E)\left(\frac{2\pi k_{vj}}{\mu}\right)^{\frac{1}{2}}\left\{\frac{\sqrt{2(1+\delta_{0,K})}}{2}\right\}e^{-ik_{vj}R_\infty}. \tag{41}$$

The equations equivalent to Eqs. (39–41) arising in the Real Wavepacket method are [41]:

$$C_{vjk}^{JK} = \left\langle \Theta_{jK}(\theta)\chi_{vj}(r)\middle|\Phi_{f,k}^{JKR}(\mathbf{r}, R=R_\infty)\right\rangle \tag{42}$$

where the superscript R in $\Phi_{f,k}^{JKR}(\mathbf{r}, R=R_\infty)$ indicates that only the real part wavepacket is used, the subscript k indicates the kth iterate (see Eq. 24) of the real part of the wavepacket and the subscript f indicates that the wavepacket is the solution of a "mapped" Schrödinger equation (see Eq. 15).

$$A_{vj}^{JK}(f) = \frac{1}{2\pi}\sum_{k=0}^{N}\left(1-\frac{\delta_{k,0}}{2}\right)\exp(ifk)\ C_{vjk}^{JK} \tag{43}$$

where $A_{vj}^{JK}(f)$ is a function of the mapped and scaled energy f (see Eq. (13)).

Taking into account now also of the factor $\frac{\mathrm{d}f}{\mathrm{d}E}$ arising from the necessary transformation of the Dirac delta function from $\delta(f-f')$ to $\delta(E-E')$ we obtain:

$$A_{vj}^{JK}(E_s) = 2\times\frac{\mathrm{d}f}{\mathrm{d}E}\frac{1}{2\pi}\sum_{k=0}^{N}\left(1-\frac{\delta_{k,0}}{2}\right)\exp(ifk)\ C_{vjk}^{JK} = \frac{1}{\sqrt{1-E_s^2}}\frac{2}{\Delta E\pi}\sum_{k=0}^{N}\left(1-\frac{\delta_{k,0}}{2}\right)\exp(ifk)\ C_{vjk}^{JK} \tag{44}$$

An extra factor of 2 has been included in Eq. (44). This arises from the analysis of "Appendix A" of Ref. [56] where it was shown that when only the real part of the wavepacket is used the $A_{vj}^{JK}(E)$ coefficients must be multiplied by this factor. This $A_{vj}^{JK}(E_s)$ coefficient may then be used in Eq. (41) to give the photofragmentation **T** matrix elements. Note that in Eq. (44) the $A_{vj}^{JK}(E_s)$ coefficient is a function of the shifted and scaled energy E_s as defined in Eq. (14).

For reference a summary of the equations needed to compute various reactive scattering and photodissociation cross sections are listed in "Appendices B and C", respectively. In particular "Appendix C" gives an expression for the detailed differential partial photodissociation cross section which is not available elsewhere in the literature and includes a phase correction to the photofragmentation **T** matrix elements arising from the fact that the centrifugal potential is not zero at the analysis line.

5 Examples

Below I will outline some examples of both reactive scattering and photodissociation calculations using wavepacket techniques. The reactive scattering calculations have all been performed using our Real Wavepacket method, which was first introduced in 1998 [56]. For photodissociation the methods used will be the standard time-dependent wavepacket methods. The Real Wavepacket formulae for photodissociation have only been recently written down in Ref. [41] and in the present paper. They should lead to important improvements in the efficiency of the codes for future applications. (See however Ref. [86] where similar methods are used).

5.1 Reactive scattering

Figure 2 shows the ratio of the total reactive cross section for the reaction $O + H_2(v = 0, j) \rightarrow OH + H$ with the reactant H_2 molecule in its $j = 1$ and $j = 2$ states [87]. The solid line is from a Real Wavepacket calculation, and it is compared with an experimentally determined value. The theoretical results, as with all wavepacket based methods, span a large range of collision energies, while the experiments were available at only a single energy. The calculations involved the use of three potential energy surfaces corresponding to three different electronic states of the system. Two of these surfaces are coupled through a conical intersection. Calculations must be performed for very many values of the total angular momentum and the results summed to obtain the cross sections (see Eq. 59). Also for the $H_2(j = 1)$ reactant, initial wavepackets with $K = 0$ and 1 must be considered. The calculations used some simplifying assumptions, namely the helicity decoupling approximation in which the coupling between different K values is ignored and not all values of J were computed. An interpolation method was used to obtain results for those values of J which were not explicitly calculated. As we can see the comparison between the theoretical results and the experiment is impressively good. This is likely to be somewhat fortuitous as we would not expect this level of agreement.

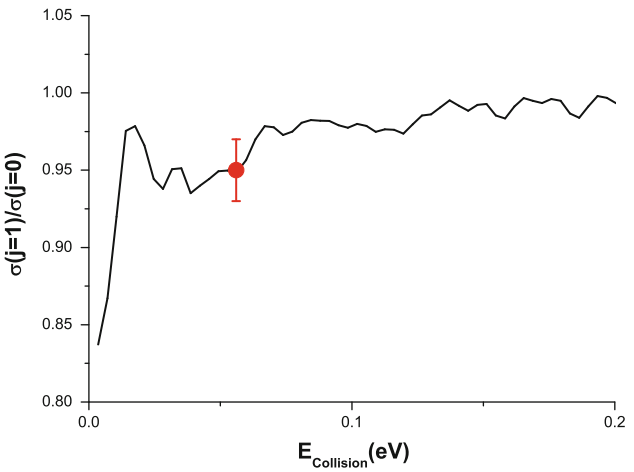

Fig. 2 Ratio of total reactive cross section for the reaction $O + H_2(v = 0, j) \rightarrow OH + H$ with the reactant H_2 molecule in its $j = 1$ and $j = 2$ states. Comparison of theory and experiment. See Ref. [87]. *Solid line* calculated using the Real Wavepacket method

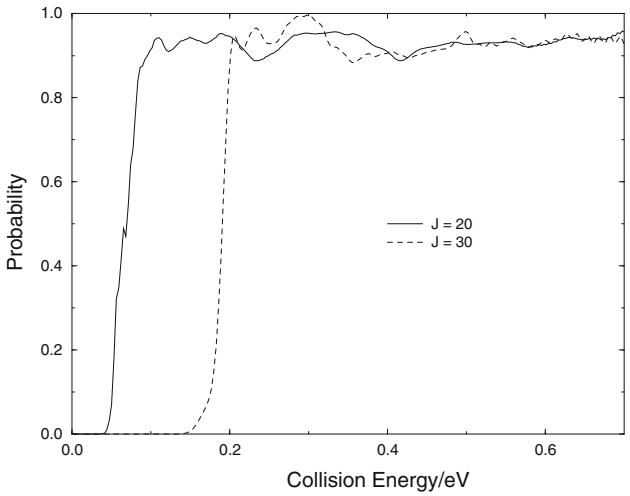

Fig. 3 Total reaction probability for $O + H_2(v = 0, j = 0) \rightarrow OH + H$ on ground state potential energy surface for different values of the total angular momentum J. See Ref. [88]

Figure 3 illustrates the important role played by the total angular momentum in determining the reaction cross section. The figure shows the total reaction probability, P_J, for two different values of J for the reaction $O + H_2$ $(v = 0, j = 0) \rightarrow OH + H$. The total reaction cross section is related to the total reaction probability by the equation:

$$\sigma(E_{\mathrm{col}}; v, j) = \frac{\pi}{k_{\mathrm{col}}^2} \frac{1}{2j+1} \sum_{J=0} (2J+1) P_J(E_{\mathrm{col}}), \tag{45}$$

There is no barrier to the reaction. Figure 3 illustrates however that the onset of the reaction occurs at progressively larger values of the collision energy for larger values of the total angular momentum, J. For any particular collision energy there is therefore a maximum value of J which can contribute. The increase in the energy onset of the reaction probability arises from the increase of the centrifugal barrier with increase in the value of J [88].

We have recently written and started to distribute a Real Wavepacket based code, DIFFREALWAVE [47, 79] for the calculation of state-to-state differential cross sections for atom-diatom reactions. Figure 4 shows the results of some calculations for the $H + H_2(v = 0, j = 0) \rightarrow H_2(v', j') + H$ differential reactive cross section using two electronic state potential energy surfaces which are

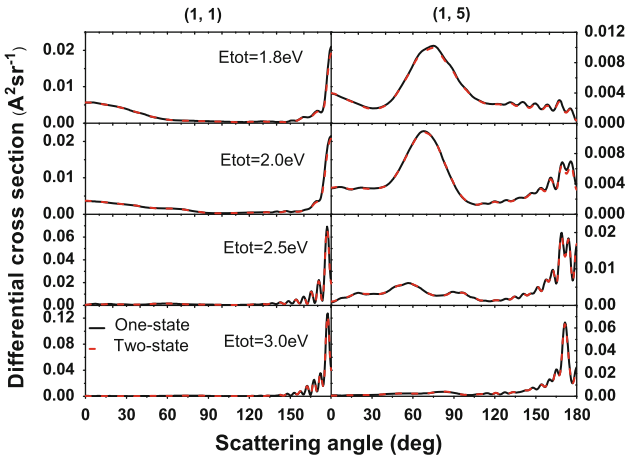

Fig. 4 State-to-state reactive differential cross sections for the reactions $H + H_2(v = 0, j = 0) \rightarrow H_2(v' = 1, j' = 1, 5) + H$ at different total energies. Two lines are shown. One corresponding to scattering on a single adiabatic potential energy surface and the other corresponding to scattering on two coupled diabatic potential energy surfaces with the cross section summed over the products scattered into the two diabatic channels. (Figure used with permission from J Chem Phys 130, 144301 (2009))

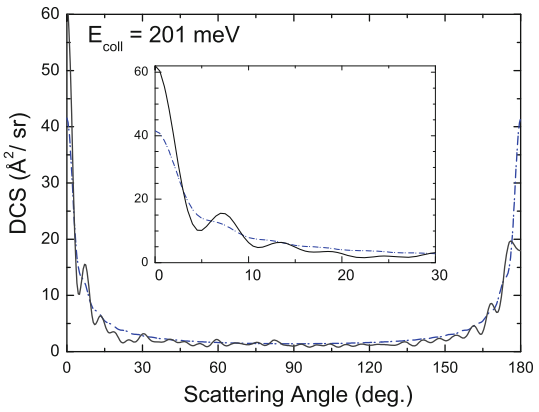

Fig. 5 Total reactive differential cross sections for the reaction $H^+ + D_2(v = 0, j = 0) \rightarrow D^+ + HD$ calculated using the "exact" Real Wavepacket method (*solid line*) and an approximate statistical quasi-classical trajectory approach (*dash-dot line*) (see Ref. [90])

connected by a conical intersection [89]. The figure also shows the result of two different calculations. One uses just a single adiabatic potential energy surface, while the other uses two coupled diabatic surfaces and the cross sections on the two diabatic surfaces are summed. The two sets of results are indistinguishable, showing that, at the energies shown, there are no detectable effects due to non-adiabaticity arising from the conical intersection.

Figure 5 shows a differential reactive cross section for the reaction $H^+ + D_2(v = 0, j = 0) \rightarrow D^+ + HD$ [90]. The figure compares the exact calculations with a statistical approximation. The reaction proceeds through a deep well and is generally assumed to be highly staticical in nature. The small differences between the results of these two calculations shows that there is a degree of non-statistical dynamics which occurs in the reaction.

5.2 Photodissociation theory

Figures 6 and 7 show *ab initio* calculations on the photodissociation of HF [91, 92]. Figure 6a shows the total photodissociation cross section for HF from its ground $v = 0$ vibrational state as a function of the energy of the light. The circles in the figure show the experimental measurements of Nee et al. [93]. Figure 6b shows the cross section for HF initially in its excited $v = 3$ vibrational state. Here we see clearly the nodal structure of the initial vibrational state mirrored in the energy dependence of the cross section.

HF can dissociate to yield either ground state, $F(^2P_{\frac{3}{2}})$, fluorine atoms or electronically excited $F(^2P_{\frac{1}{2}})$ atoms. Figure 7 shows the branching fraction $\Gamma = \sigma^*/(\sigma + \sigma^*)$ for producing excited state atoms as a function of the energy of the dissociating light [91, 92]. The *ab initio* calculations [91, 92] (solid lines) agree well with the experimental [94] measurements of these quantities. The highly structured form of the branching fraction for HF($v = 3$) (Fig. 7b) is a consequence of the structure seen in its photodissociation cross section (Fig. 6b).

The magnitude of the photodissociation cross section depends directly on the transition dipole moment. The computed value of the transition dipole in turn is very sensitive to the quality of the *ab initio* calculation. Figure 8 shows the total photodissociation cross section for the $2A' \leftarrow 1A'$ absorption in N_2O calculated using potential energy surfaces and transition dipole moment surfaces computed using different atomic orbital basis sets. All the electronic structure calculations were performed using Multi-reference configuration interaction methods [95]. It is instructive to notice that quite large atomic orbital basis sets (QZ or quadruple zeta) are needed to attain reliable results.

Figure 9 shows the calculated N_2 product rotational quantum state distribution arising from the $2A' \leftarrow 1A'$ photolysis of N_2O using light of wavelength 203.2 nm. The two parts of the figure correspond to N_2O being initially in its lowest rotational-vibrational state and in a state with one quantum of bending vibration. The theoretical rotational distributions can be compared to the those obtained experimentally from both state-selected ((010) level) [96] and non-state-selected [97] photodissociation at 203 nm which peak at $j_{max} = 74$. We see that the calculated rotational quantum state distribution from the ground rotational-vibrational state (Fig. 9a) peaks exactly at the same quantum number as observed experimentally, while photolysis of an a molecule initially with one quantum of

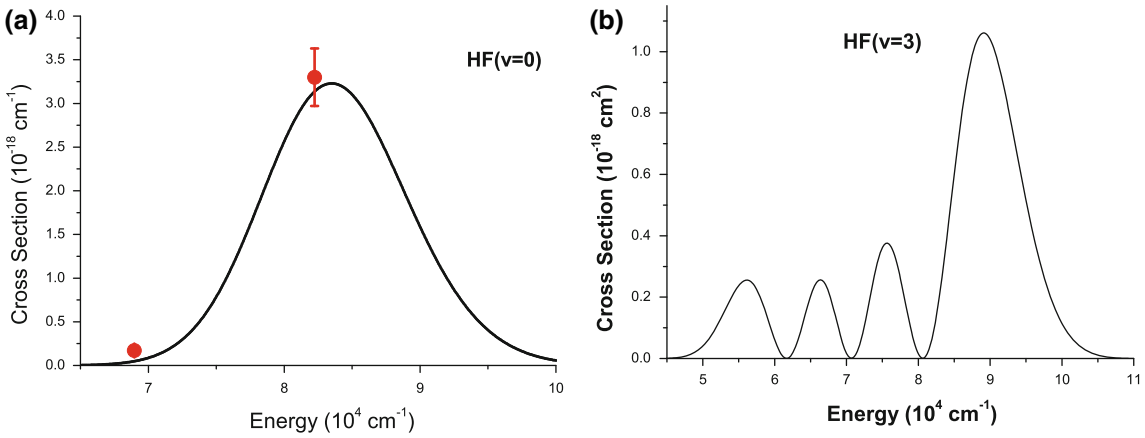

Fig. 6 Photodissocaition cross sections for HF as a function of the energy of the light used. **a** From initial vibrational state ($v = 0$). *Solid line ab initio* calculations from Ref. [91], Circles experimental results from Ref. [93]. **b** From initial vibrational state ($v = 3$). *Solid line ab initio* calculations from Ref. [92]

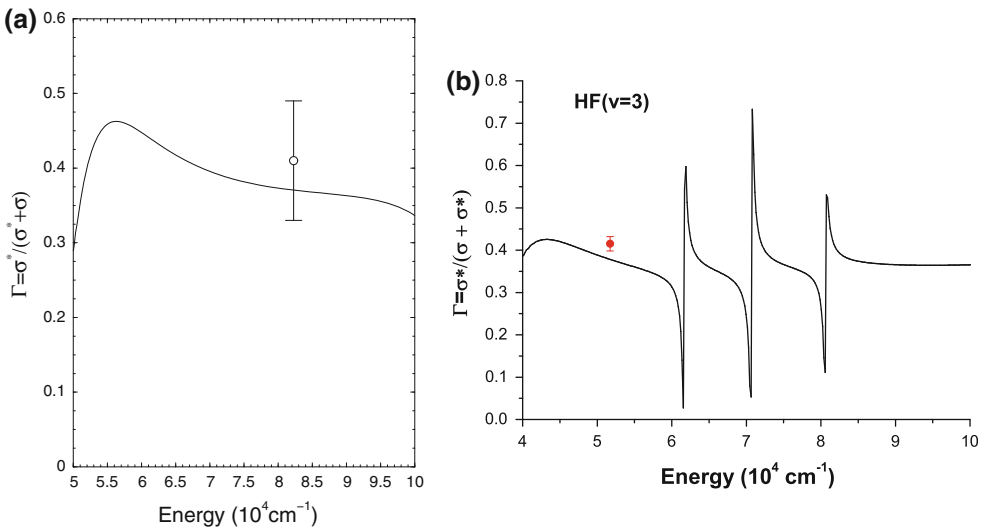

Fig. 7 Branching fractions for HF. The quantities plotted are $\Gamma = \sigma^*/(\sigma + \sigma^*)$, where σ is the cross section for producing ground state fluorine atoms, $F(^2P_{\frac{3}{2}})$, and σ^* that for producing excited state atoms, $F(^2P_{\frac{1}{2}})$. **a** Photodissociation from initial vibrational state ($v = 0$). *Solid line ab initio* calculations from Ref. [91], Circle experimental results from [94]. **b** Photodissociation from initial vibrational state ($v = 3$). *Solid line ab initio* calculations from Ref. [92]. Circle experimental results from [94]

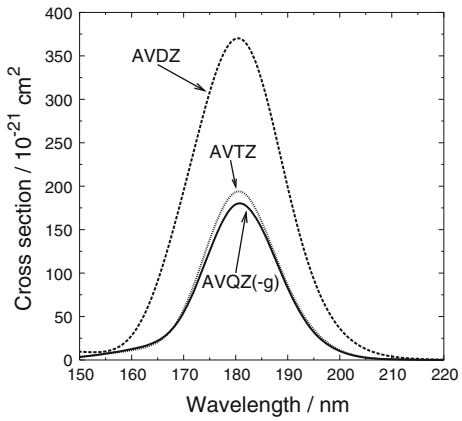

Fig. 8 $2A' \leftarrow 1A'$ cross sections using *ab initio* potential energy surfaces and transition dipole moment surfaces computed using different basis sets. *AVDZ* augmented valence double zeta, *AVTZ* augmented valence triple zeta, *AVQZ*(*-g*) augmented valence quadruple zeta minus g type Gaussian orbitals. (Reprinted with permission from Ref. [95])

bending excitation (Fig. 9b) leads to a distribution which peaks at $j_{max} = 75$. Note also the immensely greater magnitude of the cross sections when N_2O is initially in an excited bending vibrational state (Fig. 9b) when compared with those when it is initially in its ground vibrational state (Fig. 9a). This arises because the transition dipole moment is zero in the collinear electronic ground state equilibrium geometry and the absorption is entirely dependent on the bending motion of the molecule. In the ground vibrational state this bending motion is provided by the zero point motion of the bending vibration.

Figure 10 shows the calculated [98, 99] photon absorption cross section for ozone initially in its lowest vibrational-rotational state and possessing zero total angular momentum. The calculated cross section is compared with the experimentally measured [100] absorption spectrum in the region of the Hartley continuum. We see clearly that the peak of the calculated cross section occurs

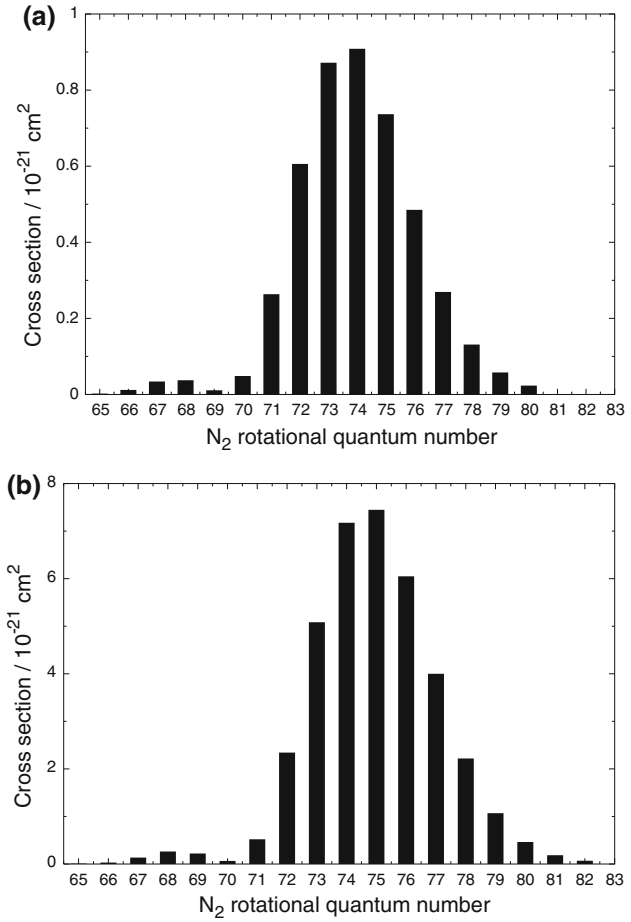

Fig. 9 Product rotational quantum state distribution resulting from the $2A' \leftarrow 1A'$ photolysis at 203 nm. N_2O initially in its (**a**) ground vibrational–rotational state; (**b**) the 010 vibrational-rotational state with one quantum of bending vibration. (Reprinted with permission from Ref. [95])

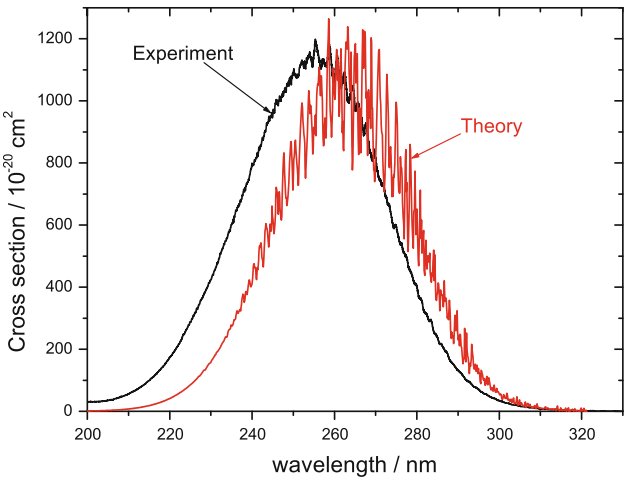

Fig. 10 Comparison of experimental [100] and theoretical [98, 99] absorption cross section of ozone in the region of the Hartley continuum. For the theoretical calculations ozone molecule was initially taken to be in its lowest vibrational-rotational state with zero total angular momentum

at a larger wavelength than the peak of the experimental absorption spectrum. This must arise from the inadequacy of the computed or numerically fitted potential energy surfaces. It is likely that the energy separation of the ground and $\tilde{B}$ state potential energy surfaces is too small in the region of the minimum of the ground state surface. Another major difference between the calculated and experimental spectra is that the theoretical absorption cross section shows far more superimposed "diffuse" structure than the experimental spectrum. This structure generally arises from part of the wavepacket becoming temporarily trapped on the excited state potential energy surface. We are still working on resolving the reason for this difference between the experimental and computed lineshapes. The calculations used only one diabatic potential energy surface for the upper electronic state. They ignored non-adiabatic transitions leading to the production of ground state O_2 molecules. This is one possible reason for the enhanced structure of the theoretical absorption spectrum as compared with the experimental one.

Figure 11 shows the calculated absorption cross section for ozone starting initially in different vibrational levels. In all cases the initial rotational angular momentum was zero. Excitation of a single quantum of the symmetric stretching motion ((100) level) results in a double peaked absorption lineshape, a broadening of the absorption spectrum to longer wavelengths and a decrease in the peak absorption strength. Excitation of the bending motion ((010) level) leads to only a very small, almost imperceptible, shift of the absorption lineshape to longer wavelengths while excitation of the asymmetric stretching motion ((001) level) results in a major reduction in the diffuse structure accompanied by a shift of the lineshape to longer wavelengths. Excitation of the asymmetric stretching motion leads to a more direct dissociation processes in which the molecule has less opportunity to become temporarily trapped on the excited state surface.

6 Conclusions

In this article I have reviewed the role of wavepackets in the theory of photodissociation. Its role in reactive scattering theory has been extensively reviewed elsewhere [36, 41]. The article discusses how, starting from a time-independent viewpoint, a time-dependent wavepacket approach can be introduced into the theory. An alternative form of the time-dependent Schrödinger equation, first introduced by Gray, [57] is then discussed. This iterative equivalent to the standard time-dependent Schrödinger equation does not

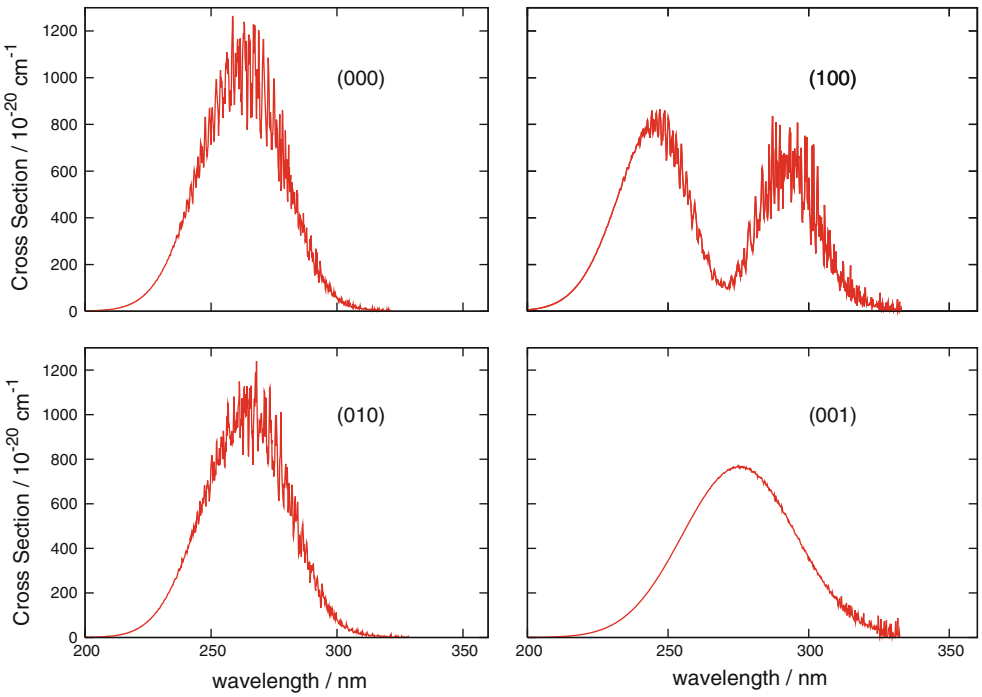

Fig. 11 Computed photon absorption cross sections for ozone starting in different initial vibrational levels. The vibrational levels are marked on the different panels. In all cases the initial total angular momentum was zero [98, 99]

involve the complex number "i" and therefore permits the separation of the real and imaginary parts of the solution. The Real Wavepacket method [56] is then discussed. The method uses a mapping of the Hamiltonian and through this circumvents the need to evaluate either $\cos(\hat{\mathbf{H}}\mathbf{t}/\hbar)$ or $\exp(-\mathbf{i}\hat{\mathbf{H}}\mathbf{t}/\hbar)$ but instead uses the Hamiltonian itself directly. The advantages of the Real Wavepacket method are that it requires overall far fewer evaluations of the action of the Hamiltonian on the wavepacket and it requires less storage, as only the real part of the wavepacket is used during the major part of the calculation.

The application of the Real Wavepacket method to the calculation of both the total integral photodissociation cross section and partial differential and integral cross sections is discussed. In the case of the partial cross sections some new equations are developed. Three appendices are presented. These cover the definition of the initial wavepacket in the photodissociation of a triatomic molecule and a summary of the equations needed for the evaluation of cross sections in both reactive scattering and photodissocaition theory when using the Real Wavepacket method.

Section 5 gives examples of the use of wavepacket calculations for both reactive scattering and photodissociation theory. The theory and its application to explaining and understanding experimental results is maturing and the constant increase in computer power is enabling progressively more exact calculations to be undertaken. An important aspect of both reactive scattering and photodissociation that has not been covered in this article is that of vector correlation and alignment. This area is at the forefront of both experimental and theoretical molecular dynamics [101–105].

Acknowledgments I would like to thank my many colleagues and friends who have collaborated with me over many years for their essential part in developing the methods outlined in this review and for performing many of the calculations used as illustrations. In particular I thank Marlies Hankel, Stephen K. Gray, Alex Brown, F. Javier Aoiz, Niyazi Bulut, Tianshu Zhu, Mohammad Noh Daud, Ezinvi Baloitcha, Richard N. Dixon, László Füsti-Molnár, Clay C. Marston, Alison Offer, George C. Schatz, Moshe Shapiro and Sean C. Smith.

Appendices

Appendix A: detailed definition of the initial wavepacket for photodissociation of a triatomic molecule

The results presented here follow the analysis presented in Ref. [80]. It is only possible to give a definition of the functions $\Phi_i^{J'K}(r,R,\theta,t=0)$ when we have specified whether the electronic transition involved is perpendicular or parallel (i.e. the transition dipole moment is perpendicular to the molecular plane or lies in the plane).

For the case of a perpendicular transition when the transition dipole is in the body-fixed y direction (perpendicular to molecular plane).

$$
\begin{aligned}
&\Phi_i^{J'K}(r,R,\theta,t=0)\\
&=\frac{i}{\sqrt{8\pi^2}}(2J_i+1)^{\frac{1}{2}}(2J_i'+1)^{\frac{1}{2}}\mu_y\delta_{p,p'}\frac{(-1)^{-(K_i)}}{\sqrt{2}}\\
&\times\sum_{K_i=\lambda}^{J_i}\psi^{J_i,K_i,p}(r,R,\theta)\\
&\times\left\{(-1)^{-1}\begin{pmatrix}1 & J_i & J'\\ 1 & K_i & -(1+K_i)\end{pmatrix}\delta_{K,K_i+1}(1-\delta_{K_i,0})\right.\\
&+\sqrt{(1+\delta_{0,(K-1)})}(-1)^{J_i+J'}\begin{pmatrix}1 & J_i & J'\\ 1 & -K_i & (K_i-1)\end{pmatrix}\\
&\times\delta_{K,K_i-1}(1-\delta_{K_i,0})\\
&\left.-(-1)^{-1}\begin{pmatrix}1 & J_i & J'\\ 1 & 0 & -1\end{pmatrix}\delta_{K,1}\delta_{K_i,0}\delta_{\lambda,0}\right\}
\end{aligned}
\tag{46}
$$

For the case of a parallel transition when the transition dipole lies in the molecular plane xz we obtain:

$$
\begin{aligned}
&\Phi_i^{J'K}(r,R,\theta,t=0)\\
&=\frac{1}{\sqrt{8\pi^2}}(2J_i+1)^{\frac{1}{2}}(2J_i'+1)^{\frac{1}{2}}\delta_{p,p'+1}\\
&\times\sum_{K_i=\lambda}^{J_i}\frac{(-1)^{-K_i}}{\sqrt{2}}\psi^{J_i,K_i,p}(r,R,\theta)\\
&\times\left\{\mu_x\left[\begin{pmatrix}1 & J_i & J'\\ 1 & K_i & -(1+K_i)\end{pmatrix}\delta_{K,K_i+1}(1-\delta_{K_i,0})\right.\right.\\
&+(-1)^{J_i+J'}\sqrt{1+\delta_{0,(K_i-1)}}\begin{pmatrix}1 & J_i & J'\\ 1 & -K_i & (K_i-1)\end{pmatrix}\\
&\left.\times\delta_{K,K_i-1}(1-\delta_{K_i,0})\right]\\
&+\begin{pmatrix}1 & J_i & J'\\ 0 & K_i & -K_i\end{pmatrix}\sqrt{2}\mu_z\delta_{K,K_i}(1-\delta_{K_i,0})\\
&+\begin{pmatrix}1 & J_i & J'\\ 1 & 0 & -1\end{pmatrix}\mu_x\delta_{K,1}\delta_{K_i,0}\delta_{\lambda,0}\\
&\left.+\begin{pmatrix}1 & J_i & J'\\ 0 & 0 & 0\end{pmatrix}\mu_z\delta_{K,0}\delta_{K_i,0}\delta_{\lambda,0}\right\}.
\end{aligned}
\tag{47}
$$

Appendix B: summary of reactive scattering formulae for the Real Wavepacket method

This appendix is a summary of the equations needed to compute the reactive differential and integral cross sections for an atom-diatom reaction. The equations are taken from Ref. [47]. An important aspect of reactive scattering is that there are two different Jacobi coordinate systems, the reactant (R^a, r^a, γ^a) and the product (R^c, r^c, γ^c) coordinates.

1. Initial wavepacket

$$
q(R^a,r^a,\gamma^a;t=0)=w(R^a-R_0)e^{-ik_0(R^a-R_0)}\varphi_{v,j}^{\mathrm{BC}}(r^a,\gamma^a). \tag{48}
$$

where $w(R^a-R_0)$ is a sinc or Gaussian [106] and $\varphi_{v,j}^{\mathrm{BC}}(r^a,\gamma^a)$ is the initial wavefunction of the reactant diatomic.

2. Transformation to product Jacobi coordinates

$$
q^{J\Omega'}(R^c,r^c,\gamma^c)=q^{J\Omega}(R^a,r^a,\gamma^a)\frac{R^c r^c}{R^a r^a}d^J_{\Omega\Omega'}(\beta). \tag{49}
$$

where $d^J_{\Omega\Omega'}(\beta)=D^J_{\Omega\Omega'}(0\beta 0)$ is a reduced Wigner rotation matrix [82, 83] and β is the angle between the vectors $\vec{R}^a$ and $\vec{R}^c$.

From this point on we work entirely in terms of product Jacobi coordinates, (R^c, r^c, γ^c) = (R, r, γ)

3. Analysis of wavepacket and calculation of differential cross sections

$$
C^J_{v,j,\Omega\to v',j',\Omega'}(t)=\int\varphi^*_{v',j'}(r,\gamma)q^{J\Omega'}(R=R_\infty,r,\gamma,t)\mathrm{d}r\mathrm{d}\gamma. \tag{50}
$$

where $\varphi^*_{v',j'}(r,\gamma)$ is an eigenfunction of the product diatomic and $q^{J\Omega'}(R=R_\infty,r,\gamma,t)$ is the real part of the wavepacket.

$$
A^J_{v,j,\Omega\to v',j',\Omega'}(E)=\frac{1}{2\pi}\int_0^\infty e^{iEt/\hbar}C^J_{v,j,\Omega\to v',j',\Omega'}(t)\mathrm{d}t. \tag{51}
$$

Body-fixed Space-fixed transformation: In order to calculate the correct phase of the S matrices we need to transform to the space-fixed coordinates, add some missing phase and then transform back.

$$
A^J_{v,j,\ell\to v',j',\ell'}(E)=\sum_{\Omega'\Omega}^{\min(j',J)}Z^J_{\ell\Omega}A^J_{v,j,\Omega\to v',j',\Omega'}(E)Z^J_{\ell'\Omega'} \tag{52}
$$

where $Z^J_{\ell'\Omega'}$ are the elements of the transformation matrix for the products and $Z^J_{\ell\Omega}$ for the reactants.

The transformation matrix with elements $Z^J_{\ell'\Omega'}$, is the matrix which diagonalises the Coriolis coupling matrix (i.e. whose columns are the eigenvector of this matrix).

The **S** matrix elements in the space-fixed coordinate system are then given by [56]:

$$
\begin{aligned}
S^J_{v,j,\ell\to v',j',\ell'}(E)=&-\frac{\hbar^2}{(1-E_s^2)^{1/2}\Delta E}\left(\frac{k_{v'j'}k_{vj}}{\mu_r\mu_p}\right)^{1/2}\\
&\times\frac{2A^J_{v,j,\ell\to v',j',\ell'}(E)}{\bar{g}(-k_{vj})}e^{-i\left(k_{v'j'}R_\infty+\delta\eta_{v'j'\ell'}+\delta\eta_{vj\ell}\right)}
\end{aligned}
\tag{53}
$$

where E_s is the scaled and shifted energy corresponding to the energy E, μ_r and μ_p are the reduced masses for the scattering coordinates in the reactant and product Jacobi coordinates respectively. $k_{v'j'}$ is the wavevector component associated with the product channel and is calculated as

$$
k_{v'j'}=\sqrt{2\mu_p\left(E-\left(\varepsilon_{v'j'}+\frac{\ell'(\ell'+1)}{2\mu_pR_\infty^2}\right)\right)}. \tag{54}
$$

The quantities $\delta\eta_{v'j'\ell'}$ and $\delta\eta_{v\ j\ \ell}$ in Eq. (53) are phase corrections that arise because the centrifugal potential is

not zero at the analysis line. The correction to the phase in the exit channel is:

$$\delta\eta_{v'j'\ell'} = \int_{R_\infty}^{\infty} dR\left\{\sqrt{2\mu_p\left(E-\varepsilon_{v'j'}-\frac{\ell'(\ell'+1)}{2\mu_p R^2}\right)} - \sqrt{2\mu_p\left(E-\varepsilon_{v'j'}\right)}\right\} \tag{55}$$

while in the entrance channel the equivalent correction is:

$$\delta\eta_{vj\ell} = \int_{R_0}^{\infty} dR\left\{\sqrt{2\mu_r\left(E-\varepsilon_{vj}-\frac{\ell(\ell+1)}{2\mu_r R^2}\right)} - \sqrt{2\mu_r\left(E-\varepsilon_{vj}\right)}\right\}. \tag{56}$$

The integrals in Eqs. (55) and (56) can be performed analytically [47].

Having calculated the **S** matrix in the space-fixed basis we now transform back to the body-fixed basis.

$$S^J_{v,j,\Omega\to v',j',\Omega'}(E) = \sum_{\ell'\ell} Z^J_{\Omega\ell} S^J_{v,j,\ell\to v',j',\ell'}(E) Z^J_{\Omega'\ell'} \tag{57}$$

The differential cross section is then given by [36, 84]:

$$\sigma(E,\theta,v,j\to v',j') = \frac{1}{2j+1} \times \sum_{\Omega'\Omega}\frac{1}{4k^2_{vj}}\left|\sum_J (2J+1) S^J_{v,j,\Omega\to v',j',\Omega'}(E) d^J_{\Omega\Omega'}(\theta)\right|^2. \tag{58}$$

The state-to-state integral cross section is given by:

$$\sigma(E,v,j\to v',j') = \frac{\pi}{k^2_{vj}}\frac{1}{2j+1}\sum_{\Omega'\Omega} \times \sum_J (2J+1)\left|S^J_{v,j,\Omega\to v',j',\Omega'}(E)\right|^2. \tag{59}$$

Appendix C: summary of photodissociation theory formulae for the Real Wavepacket method

This appendix is a summary of the equations needed to compute the photodissociation cross sections arising in the photodissociation of a triatomic molecule. The equations are derived in the present paper and in Refs. [36, 80, 41].

1. Total integral photodissociation cross section

$$\sigma_{tot}(E) = \frac{1}{\Delta E\sqrt{1-E_s^2}}\frac{8\pi v}{c\epsilon_0}\sum_{J=J_i-1}^{J_i+1}\sum_{K=\lambda}^{J}\sum_{k=0}^{N}\left(1-\frac{\delta_{k,0}}{2}\right) \times \exp(ifk)\left\langle \Phi^{JKR}_{f,k=0}(\mathbf{r},R)|\Phi^{JKR}_{f,k}(\mathbf{r},R)\right\rangle \tag{60}$$

See Eqs. (13) and (14) for meaning of f, the mapped energy.

2. Partial cross sections and final state analysis

$$C^{JK}_{vjk} = \left\langle \Theta_{jK}(\theta)\chi_{vj}(r)\middle|\Phi^{JKR}_{f,k}(\mathbf{r},R=R_\infty)\right\rangle \tag{61}$$

see Eq. (42).

$$A^{JK}_{vj}(E_s) = \frac{1}{\sqrt{1-E_s^2}}\frac{2}{\Delta E\pi}\sum_{k=0}^{N}\left(1-\frac{\delta_{k,0}}{2}\right)\exp(ifk)C^{JK}_{vjk} \tag{62}$$

see Eq. (44) and see Eq. (14) for a definition of the shifted and scaled energy, E_s.

The photofragmentation **T** matrix elements are:

$$T^{JKp}_{vj} = i(-1)^{K-j}A^{JK}_{vj}(E)\left(\frac{2\pi k_{vj}}{\mu}\right)^{\frac{1}{2}}\left\{\frac{\sqrt{2(1+\delta_{0,K})}}{2}\right\}e^{-ik_{vj}R_\infty}. \tag{63}$$

Phase Corrections:

By analogy with the reactive scattering case it is clear that a phase correction will be needed for the photofragmentation **T** matrix elements to take account of the fact that the analysis line may not be sufficiently far out for the centrifugal barrier and coupling to be negligible. Making an analogy with Eq. (52), Ω' in Eq. (52) has the same meaning as K in Eq. (63). We may therefore transform the photofragmentation **T** matrix from the body-fixed to the space-fixed coordinate frame using:

$$T^{J\ell p}_{vj} = \sum_{K}^{\min(j,J)} T^{JKp}_{vj} Z^J_{\ell K} \tag{64}$$

Now apply phase correction (see Eq. (55)).

$$\bar{T}^{J\ell p}_{vj} = T^{J\ell p}_{vj} e^{-i\delta\eta_{vj\ell}} \tag{65}$$

and then transform back to the body-fixed frame to obtain the corrected photofragmentation $\bar{\mathbf{T}}$ matrix elements:

$$\bar{T}^{JKp}_{vj} = \sum_{K}^{\min(j,J)} \bar{T}^{J\ell p}_{vj} Z^J_{K\ell} \tag{66}$$

The state-to-state photofragmentation differential cross section is then given by (see Eq. 33):

$$\sigma_{vjm_j}(E,\hat{\mathbf{k}}) = \frac{2\pi^2 v}{c\epsilon_0}\left|(-1)^{m+M_i}\sum_{J=J_i-1}^{J_i+1} \times \sum_{lm_l} Y^*_{lm_l}(\hat{\mathbf{k}})(jlJ(M_i+m)|jm_j lm_l)\sum_{K=\lambda}^{J}(Jjl0|JKj-K) \times \begin{pmatrix} 1 & J_i & J \\ m & M_i & -(m+M_i)\end{pmatrix}\bar{T}^{JKp}_{vj}\right|^2 \tag{67}$$

where $\hat{\mathbf{k}}$ represents the direction in the laboratory reference frame into which the scattering takes place. Note that both

the initial M_i state and the final m_j state are specified in this expression and that these magnetic quantum numbers have not been summed or averaged over.

We can sum over all m_j product states and integrate over all scattering angles to obtain the state-to-state integral photofragmentation cross section (see Eq. 37):

$$\bar{\sigma}_{vj}(E) = \frac{2\pi^2 \nu}{c\epsilon_0} \sum_{J=J_i-1}^{J_i+1} \sum_{K=\lambda}^{J} \left| \begin{pmatrix} 1 & J_i & J \\ m & M_i & -(m+M_i) \end{pmatrix} T_{vj}^{JKp} \right|^2 \tag{68}$$

This cross section is for the molecule initially in the rotational state J_i, M_i and m represents the spherical vector polarization direction of the photodissociating light.

The integral photofragmentation cross section averaged over initial M_i states and summed over final m_j states can be found by averaging Eq. (68) over M_i states using Eq. (3.7.8) of Ref. [82].

$$\bar{\bar{\sigma}}_{vj}(E) = \frac{1}{(2J_i+1)} \frac{2\pi^2 \nu}{3c\epsilon_0} \sum_{J=J_i-1}^{J_i+1} \sum_{K=\lambda}^{J} \left| T_{vj}^{JKp} \right|^2 \tag{69}$$

Reference [81] describes the different detailed cross sections and their interrelationships. Taking the sum of the partial cross sections in Eq. (69) over all final state quantum numbers should give the same total photoabsorption cross section as in Eq. (60). As these two quantities are calculated in completely different ways this provides a valuable internal check of the calculations.

References

1. Mazur J, Rubin RJ (1959) J Chem Phys 31:1395
2. McCullough EA, Wyatt RE (1969) J Chem Phys 51:1253
3. McCullough EA, Wyatt RE (1971) J Chem Phys 54:3578
4. Zuhrt C, Kamal T, Zulicke L (1975) Chem Phys Lett 36:396
5. Kellerhals NSE, Raff L (1976) J Chem Phys 64:818
6. Agrawal PM, Raff LM (1981) J Chem Phys 74:5076
7. Leforestier C (1984) Chem Phys 87:241
8. Zhang ZH, Kouri DJ (1986) Phys Rev A 34:2687
9. Lester WA Jr (1976) In: Miller WH (ed) Modern theoretical chemistry, Vol 1. Plenum Press, New York, pp 1–32
10. Miller WH (1969) J Chem Phys 50:407
11. Wolken JG, Miller WH, Karplus M (1972) J Chem Phys 56:4930
12. Wolken JG, Karplus M (1974) J Chem Phys 60:351
13. Schatz GC, Kuppermann A (1976) J Chem Phys 65:4642
14. Schatz GC, Kuppermann A (1976) J Chem Phys 65:4668
15. Mielke SL, Lynch GC, Truhlar DG, Schwenke DW (1994) J Phys Chem 98:8000
16. Heller EJ (1978) J Chem Phys 68:2066
17. Heller EJ (1978) J Chem Phys 68:3891
18. Kulander KC, Heller EJ (1978) J Chem Phys 69:2439
19. Heller EJ (1981) Accounts Chem Res 14:368
20. Lee S-Y, Heller EJ (1982) J Chem Phys 76:3035
21. Ben-Nun M, Quenneville J, Martinez T (2000) J Phys Chem A 104:5161
22. Virshup AM, Punwong C, TVP, Lindquist BA, Ko C, Martinez T (2009) J Phys Chem B 113:3280
23. Chen X, Batista VS (2006) J Chem Phys 125:124313
24. Justin K, Wu Y, BJ-L, Batista VS (2009) Israel J Chem 49:187
25. Iyengar SS, Sumner I, Jakowski J (2008) Phys J Chem B 112:7601
26. Iyengar SS (2009) Internat J Quant Chem 109:3798
27. Feit M, JAF Jr, Steiger A (1982) J Comp Phys 47:412
28. Feit MD, Fleck JJA (1983) J Chem Phys 78:301
29. Kosloff D, Kosloff R (1983) J Comp Phys 52:35
30. Kosloff R (1988) J Phys Chem 92:2087
31. Tal-Ezer H, Kosloff R (1984) J Chem Phys 81:3967
32. Kosloff D, Kosloff R (1986) J Comp Phys 63:363
33. Kouri DJ, Mowrey RC (1987) J Chem Phys 86:2087
34. Balint-Kurti GG, Dixon RN, Marston CC (1992) Internat Rev Phys Chem 11:317
35. Jackson B (1995) Annu Rev Phys Chem 46:251
36. Balint-Kurti GG (2003) Adv Chem Phys 128:249
37. Meyer H-D, Worth GA (2003) Theoret Chem Acct 109:251
38. Althorpe SC (2004) Int Rev Phys Chem 23:219
39. Balint-Kurti GG, Brown A (2004) In: Lagana A, Lendvay G (eds) Theory of chemical reaction dynamics; Proceedings of the Nato advanced research workshop on the theory of dynamics of elementary chemical reactions. Kluwer Academic Publishers, New York, pp 149–185, ISBN 1-4020-2055-4
40. Chu T-S, Zhang Y, Han K-L (2006) Int Rev Phys Chem 25:201
41. Balint-Kurti GG (2008) Internat Rev Phys Chem 27:507
42. Goldstein H (1950) Classical mechanics. Addison-Wesley Publishing Co., Reading
43. Dirac PAM (1958) The principles of quantum mechanics, 4th ed. Clarendon Press, Oxford
44. Marston CC, Balint-Kurti GG (1990) J Chem Phys, Phys Chem Chem Phys 91
45. Balint-Kurti GG, Dixon RN, Marston CC (1990) J Chem Soc Faraday Trans 86:1741
46. Hankel M, Balint-Kurti GG, Gray SK (2001) J Phys Chem 105:2330
47. Hankel M, Smith SC, Allan RJ, Gray SK, Balint-Kurti GG (2006) J Chem Phys 125:164303
48. Huang Y, Zhou W, Kouri DJ, Hoffman DK (1993) Chem Phys Lett 206:96
49. Kouri D, Arnold M, Hoffman D (1993) Chem Phys Lett 203:166
50. Hoffman DK, Huang Y, Zhu W, Kouri DJ (1994) J Chem Phys 101:1242
51. Zhu W, Huang Y, Kouri DJ, Arnold M, Hoffman DK (1994) Phys Rev Lett 72:1310
52. Kouri DJ, Huang Y, Zhu W, Hoffman DK (1994) J Chem Phys 100:3662
53. Kouri DJ, Hoffman DK (1995) Few-Body Syst 18:203
54. Kouri DJ, Zhou W, Huang Y, Hoffman DK (1996). In: Wyatt RE, Zhang JZH (eds) Dynamics of molecules and chemical reactions. Dekker, New York
55. Althorpe SC, Kouri DJ, Hoffman DK, Moiseyev N (1997) Chem Phys 217:289
56. Gray SK, Balint-Kurti GG (1998) J Chem Phys 108:950
57. Gray SK (1992) J Chem Phys 96:6543
58. Gray SK, Verosky J (1994) J Chem Phys 100:5011
59. Gray SK, Manolopoulos D (1996) J Chem Phys 104:7099
60. Mandelshtam VA, Taylor HS (1995) J Chem Phys 103:2903
61. Vibók Á, Balint-Kurti GG (1992) J Phys Chem 96:8712
62. Vibók Á, Balint-Kurti GG (1992) J Chem Phys 96:7615
63. Chen R, Guo H (1996) J Chem Phys 105:3569
64. Mandelshtam VA, Taylor HS (1995) J Chem Phys 102:7390
65. Jang HW, Light JC (1995) J Chem Phys 102:3262
66. Kroes G-J, Neuhauser D (1996) J Chem Phys 105:8690
67. Chen R, Guo H (1996) Chem Phys Lett 261:605

68. Kroes G-J, van Hemert MC, Billing GD, Neuhauser D (1997) Phys Rev Lett 78:3583
69. Guo H, Seideman T (1999) Phys Chem Chem Phys 1:1265
70. Lin SY, Guo H, (2005) J Chem Phys 122:074304
71. Neuhauser D (1990) J Chem Phys 93:2611
72. Neuhauser D (1990) J Chem Phys 93:7836
73. Huang Y, Iyengar SS, Kouri DJ, Hoffman DK (1996) J Chem Phys 105:927
74. Neuhauser D, Judson RS, Baer M, Kouri DJ (1997) J Chem Soc Faraday Trans 93:727
75. Althorpe SC (2001) J Chem Phys 114:1601
76. Neuhauser D, Baer M, Judson RS, Kouri DJ (1990) J Chem Phys 93:312
77. Neuhauser D (1992) Chem Phys Letts 200:173
78. Meijer AJHM, Goldfield EM, Gray SK, Balint-Kurti GG (1998) Chem Phys Lett 293:270
79. Hankel M, Smith SC, Gray SK, Balint-Kurti GG (2008) Comput Phys Commmun 179:569
80. Balint-Kurti GG, Füsti-Molnár L, Brown A (2001) Phys Chem Chem Phys 3:702
81. Balint-Kurti GG, Shapiro M (1981) Chem Phys 61:137
82. Edmonds AR (1960) Angular momentum in quantum mechanics. Princeton University Press, Princeton
83. Zare RN (1988) Angular momentum. Wiley, New York
84. Balint-Kurti GG (1975) In: Buckingham AD, Coulson CA (eds) International review of science, series II, Vol. 1. Butterworth, London, pp 286–326
85. A mistake has been found in the formulae of appendix B of Ref. 36. The correct formulae are given in appendix A of this paper
86. Qu ZW, Zhu H, Grebenshchikov SY, Schinke R (2005) J Chem Phys 123:074305
87. Gray SK, Balint-Kurti GG, Schatz GC, Lin JJ, Liu X, Harich S, Yang X (2000) J Chem Phys 113:7330
88. Gray SK, Goldfield EM, Schatz GC, Balint-Kurti GG (1999) Phys Chem Chem Phys 1:1141
89. Chu T-S, Han K-L, Hankel M, Balint-Kurti GG, Kuppermann A, Abrol R (2009) J Chem Phys 130:144301
90. Jambrina PG, Aoiz FJ, Bulut N, Smith SC, Balint-Kurti GG, Hankel M (2010) Phys Chem Chem Phys 12:1102
91. Brown A, Balint-Kurti GG (2000) J Chem Phys 113:1870
92. Brown A, Balint-Kurti GG (2000) J Chem Phys 113:1879
93. Nee JB, Suto M, Lee LC (1985) J Phys B 18:L293
94. Zhang J, Riehn CW, Dulligan M, Wittig C (1996) J Chem Phys 104:7027
95. Daud MN, Balint-Kurti GG, Brown A (2005) J Chem Phys 122:054305
96. Teule JM, Groenenboom GC, Neyer DW, Chandler DW, Janssen MHM (2000) Chem Phys Lett 320:177
97. Hanisco TF, Kummel AC (1993) J Phys Chem 97:7242
98. Baloïtcha E, Balint-Kurti GG (2005) J Chem Phys 123:014306
99. Baloïtcha E, Balint-Kurti GG (2008) J Chem Phys 128:089901
100. Freeman DE, Yoshino K, Esmond JR, Parkinson WH (1984) Planet Space Sci 32:239
101. Balint-Kurti GG, Orr-Ewing AJ, Beswick JA, Brown A, Vasyutinskii OS (2002) J Chem Phys 116:10760
102. Rakitzis TP, Samartzis PC, Toomes RL, Kitsopoulos TN, Brown A, Balint-Kurti GG, Vasyutinskii OS, Beswick JA (2003) Science 300:1936
103. Brown A, Balint-Kurti GG, Vasyutinskii OS (2004) J Phys Chem 108:7790
104. Kuznetsov VV, Vasyutinskii OS (2005) J Chem Phys 123:034307
105. Balint-Kurti GG, Vasyutinskii OS (2009) J Phys Chem 113:14281
106. Hankel M, Balint-Kurti GG, Gray SK (2003) Int J Quant Chem 92:205